

High-resolution infrared spectroscopy of HCF in the CH stretch region

Cite as: J. Chem. Phys. **152**, 014305 (2020); <https://doi.org/10.1063/1.5133397>

Submitted: 23 October 2019 • Accepted: 07 December 2019 • Published Online: 03 January 2020

 Kirstin D. Doney,  Andrew Kortyna and  David J. Nesbitt

COLLECTIONS

Paper published as part of the special topic on [JCP Editors' Choice 2019](#)



View Online



Export Citation



CrossMark

ARTICLES YOU MAY BE INTERESTED IN

[High-resolution infrared spectroscopy of jet cooled CH₂Br radicals: The symmetric CH stretch manifold and absence of nuclear spin cooling](#)

The Journal of Chemical Physics **152**, 134305 (2020); <https://doi.org/10.1063/5.0002165>

[Femtochemistry under scrutiny: Clocking state-resolved channels in the photodissociation of CH₃I in the A-band](#)

The Journal of Chemical Physics **152**, 014304 (2020); <https://doi.org/10.1063/1.5134473>

[A uniform flow-cavity ring-down spectrometer \(UF-CRDS\): A new setup for spectroscopy and kinetics at low temperature](#)

The Journal of Chemical Physics **151**, 244202 (2019); <https://doi.org/10.1063/1.5125574>



Chemical Physics Reviews

First Articles Now Online!

READ NOW >>>



High-resolution infrared spectroscopy of HCF in the CH stretch region

Cite as: J. Chem. Phys. 152, 014305 (2020); doi: 10.1063/1.5133397

Submitted: 23 October 2019 • Accepted: 7 December 2019 •

Published Online: 3 January 2020



View Online



Export Citation



CrossMark

Kirstin D. Doney,^{1,a)}  Andrew Kortyna,²  and David J. Nesbitt^{2,3,4} 

AFFILIATIONS

¹JILA, National Institute of Standards and Technology, University of Colorado, Boulder, Colorado 80309-0440, USA

²JILA, University of Colorado, Boulder, Colorado 80309-0440, USA

³Department of Chemistry, University of Colorado, Boulder, Colorado 80309-0440, USA

⁴Department of Physics, University of Colorado, Boulder, Colorado 80309-0440, USA

^{a)}Electronic mail: Kirstin.Doney@jila.colorado.edu

ABSTRACT

We present the results from a high-resolution infrared study of jet-cooled singlet monofluorocarbene (HCF) in the CH stretch region near 2600 cm^{-1} . Absorption signals are recorded using near quantum shot noise limited laser absorption methods. The fully resolved absorption spectra of the CH stretch (ν_1) fundamental band and a partial progression of transitions of the HCF bend plus CF stretch ($\nu_2 + \nu_3$) combination band are observed and show clear evidence of a strong rovibrational coupling between the ν_1 $K'_a = 2$ and $\nu_2 + \nu_3$ $K'_a = 3$ manifolds, including the observation of “dark state” transitions. A detailed perturbation analysis of a c-type Coriolis interaction is carried out for these two coupled vibrational states, providing experimental determination of precise rovibrational constants. A combined ground state combination difference fit of the transitions to the ν_1 and $\nu_2 + \nu_3$ vibrational states in this study with previously reported LIF $\tilde{A}(0,0,0) \leftarrow \tilde{X}(0,0,0)$ data has been done to increase the accuracy of the ground state rotational constants [M. Kakimoto *et al.*, J. Mol. Spec. **88**, 300–310 (1981)]. Moreover, we report, for the first time, hot band ($\nu_1 + \nu_3 \leftarrow \nu_3$) transitions due to vibrationally excited HCF in the CF stretch mode, ν_3 . The high-resolution results for all vibrational frequencies and rotational constants are in good agreement with and significantly extend the analysis of the rovibrational manifold of HCF. The present ground state and ν_3 spectroscopic parameters now permit improved predictions for pure rotational and ν_3 fundamental transitions to aid spectral searches for HCF in the laboratory and the interstellar medium.

<https://doi.org/10.1063/1.5133397>

I. INTRODUCTION

Halogenated molecules are of importance to their involvement in commercial products, atmospheric and interstellar chemistry, and organic synthesis.^{5–7} In particular, halogen containing complex organic molecules (COMs, e.g., CH_3Cl) can be formed as the byproduct of biological activity and have been proposed as biomarkers in exoplanet atmospheres.⁸ However, the recent observation of CH_3Cl toward a sunlike star forming region and in the comet 67P/Churyumov-Gerasimenko indicates that there are nonbiological formation mechanisms in the interstellar medium (ISM).⁹ One such method is halogen atom, X, incorporation into simple molecules and COMs in irradiated ice mantles of dust grains, including sequential H-atom addition to CX.^{7,10}

In order to better understand how halogenated molecules are formed in the ISM, a complete understanding of the reaction-pathway intermediates and their relative abundances is needed. This requires gas-phase laboratory spectra with which unambiguous molecular assignments in astronomical observations of possible halogen containing molecules in the reaction network are made.

To date, the pure rotational transitions of three fluorinated molecules have been detected in astronomical spectra: CF^+ and HF, in diffuse and translucent clouds; HF, in dense sources;^{11–14} and HF and AlF, in circumstellar envelopes of carbon rich stars.^{15,16} HF has also been observed in absorption in interstellar gas through its infrared rovibrational transitions, $\nu = 1-0$ R(0) and R(1).¹⁷ Since the interstellar formation mechanism for CH_3F , like CH_3Cl , is thought

to be dominated by grain surface reactions starting from CF, with the diradical halocarbene HCF as an intermediate,⁷ and given that the interstellar abundance of F is comparable to Cl,¹⁸ it is highly likely that CH₃F and its simpler radical derivatives, e.g., HCF, also exist in astronomical environments. The detection of fluorinated molecules with more than two atoms is currently hampered by limited laboratory-based high resolution spectroscopic data.

The triatomic, near-prolate asymmetric top molecule (Fig. 1), HCF (\tilde{X}^1A'), has three vibrational modes: the CH stretch (ν_1 ; A') at $\sim 2643\text{ cm}^{-1}$, the HCF bend (ν_2 ; A') at $\sim 1403\text{ cm}^{-1}$, and the CF stretch (ν_3 ; A') at $\sim 1192\text{ cm}^{-1}$.^{2,3} Hereafter, the vibrational levels are denoted as (ν_1, ν_2, ν_3) , and a summary of the vibrational modes available from the literature is given in Table I. Historically, the spectroscopic data for HCF have been obtained through observation of its $\tilde{A}^1A''-\tilde{X}^1A'$ electronic transitions in studies looking for the adiabatic energy gap between its singlet ground state and the nearby triplet state and to investigate the rovibronic Renner-Teller effects.^{1,3,19-21} Conversely, the vibrational manifolds of the ground electronic state have been far less thoroughly studied. Eighteen fundamental and combination vibrational states of HCF have been observed at a relatively low resolution with stimulated emission pumping (SEP) spectroscopy by Mukarakate *et al.*²² This SEP study provides a majority of the experimental knowledge of the vibrational energy levels in the ground electronic state, complete with estimates of the vibrational energy, ν_0 , the primary rotational constant, A , and the average value for the other two rotational constants, \bar{B} . Of the known vibrational states of HCF, only four— $(0,0,0)$,¹ $(1,0,0)$, $(0,1,0)$, and $(0,2,0)$ ³—have been studied with rotationally resolved laser induced fluorescence (LIF) and SEP spectroscopy, respectively, resulting in precise determination of ν_0 , A , B , and C for each state. Based on the determined rotational constants, Suzuki and Hirota³ found a negative anharmonicity for ν_2 , which is believed to be the result of strong Fermi mixing between at least the $(1,0,0)$ and $(0,2,0)$ states.

HCF has also been the subject of numerous theoretical studies in regards to its the singlet-triplet separation (see Ref. 4 and references therein). The theoretical study by Weis *et al.*,⁴ using highly correlated coupled electron pair approach (CEPA) electronic wave functions to calculate the three-dimensional potential energy functions, predicts the vibrational energies (for states $< 6000\text{ cm}^{-1}$) with both a perturbative and a variational method. Based on the comparison with the known experimental vibrational band origins, it was determined that the variational method was the more accurate choice. However, the full extent of the interactions between the

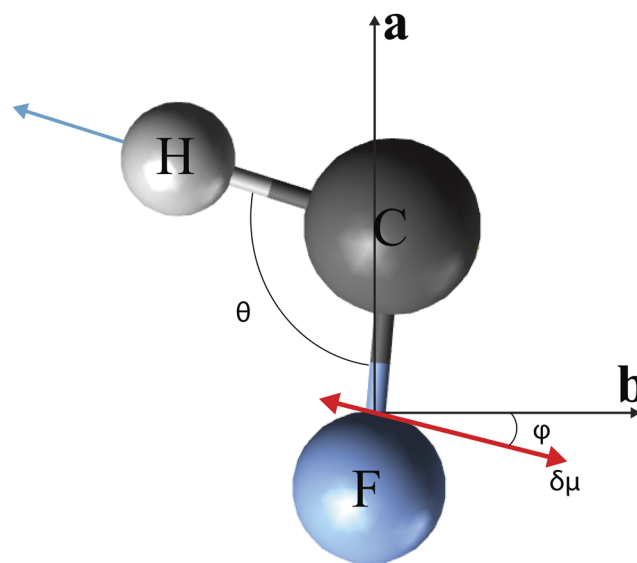


FIG. 1. The HCF CCSD(T)/cc-pCVQZ equilibrium structure and vibrational motion of the $(1,0,0)$ mode (blue arrow). The molecule lies in the plane of the principal rotation axes a and b , and the c -axis that has the largest moment of inertia is directed into the page. Here, θ is the H–C–F bond angle and ϕ is the angle between the b principal rotation axis and the direction of the CH transition dipole moment, $\delta\mu$.

$(1,0,0)$, $(0,1,1)$, and $(0,2,0)$ states still requires more experimental information, ideally through rotationally resolved absorption studies in the infrared.

In this paper, we present the high resolution experimental spectrum of gas-phase HCF around $3\ \mu\text{m}$ and the measurement of the $(1,0,0) \leftarrow (0,0,0)$, $(0,1,1) \leftarrow (0,0,0)$, and $(1,0,1) \leftarrow (0,0,1)$ rovibrational bands. This paper is organized as follows: in Sec. II, we describe the experimental approach. The experimental spectrum is presented in Sec. III along with the spectral analysis. In Sec. IV, the vibrational assignments are discussed, including a detailed perturbation analysis of the $(1,0,0)$ and $(0,1,1)$ vibrational states and comparison with *ab initio* values. Finally, the astronomical implications of the data, including predictions of possible microwave transitions, and a short conclusion are presented. Line positions are available in the [supplementary material](#).

TABLE I. A summary of the vibrational energies and vibration-rotation interaction constants (in cm^{-1}) of HCF.

Mode	Observed frequency ^a	Vib-rot interaction constants ^b		
		α_i^A	α_i^B	α_i^C
ν_1 CH str.	2643.0393	0.337(0.623)	0.0003(-0.003)	0.003(-0.001)
ν_2 bend	1403.2045	-0.372(-0.365)	-0.0003(0.0002)	0.005(0.005)
ν_3 CF str.	1192	(0.044)	(0.015)	(0.016)

^aFrom Refs. 2 and 3.

^bExperimental values from Ref. 3, and *ab initio* values from Ref. 4 are given in parentheses.

II. EXPERIMENTAL METHODS

The experimental setup has been described in detail in Ref. 23 and has recently been used to measure the CH fundamental band of the halocarbene HCCl in Ref. 24. In the present experiment, HCF radicals are generated in a supersonically expanding pulsed planar plasma using a precursor gas mixture of 0.12% fluoroform (HCF₃) in Ne (63%), He (27%), and H₂ (9%) with a 250 Torr backing pressure. The gas is expanded into a vacuum chamber through a long, thin (0.3 × 40 mm, 1 ms opening time, and 19 Hz repetition rate) slit discharge nozzle with an applied negative high voltage square wave (~7000 V/cm) modulated at 50 kHz; the resulting plasma pulse lasts for about 700 μs. In the discharge region, the precursor molecules undergo electron impact dissociation, leading to the formation of HCF from HCF₃.

To detect the molecules in the expansion, a frequency stabilized single mode ring dye laser (Spectra-Physics 380A, R6G dye) is mixed with a single mode Ar⁺ laser (Spectra-Physics Series 2000, 515 nm) in a temperature-controlled periodically poled MgO:LiNbO₃ crystal (PPLN) to generate the required narrow-band continuous wave (cw) IR light source (5–10 μW, tunable from ~2600–4600 cm⁻¹) via difference frequency generation. A dichroic mirror after the PPLN splits the IR laser light into a signal beam, which is directed to a 16-pass Herriott cell, and a reference beam. Both beams are focused onto balanced liquid-N₂ cooled InSb detectors, with their outputs electronically subtracted in a fast, home-built subtractor circuit (30 dB suppression dynamic range, 1 MHz bandwidth) to eliminate common mode amplitude noise. The integrated noise level is further reduced to near quantum shot noise levels by phase sensitive lock in detection at the discharge modulation frequency.

The high resolution IR spectrum of the plasma products is recorded using a direct absorption spectroscopy scheme, wherein the IR signal beam is multiplexed with Herriott cell optics and intersects the expansion <1 cm downstream from the nozzle body resulting in an absorbance path length of about 64 cm. To determine the relative line positions of the HCF CH stretch fundamental band, an initial rapid scan spectrum is recorded at low

signal-to-noise, with four averages per point and 20 MHz between data points to cover a total range of ~100 cm⁻¹. This region is then rescanned piecewise at higher signal-to-noise (eight averages per point and 12.5 MHz between data points). Frequencies and uncertainties are determined from repeated (3×) scans over the same transitions, and frequency precision is provided via interpolation of dye laser fringes through the Fabry-Pérot cavity locked to a stabilized HeNe laser.²⁵ The absolute frequencies are obtained by calibration against the $\nu_1 \leftarrow 0 P(9)$ transition of HCl,²⁶ resulting in a typical frequency accuracy of better than 10 MHz (0.0003 cm⁻¹). Collisional collimation in the slit jet expansion suppresses the Doppler line width to about 60 MHz, and the experimental signal-to-noise ratio for the strongest infrared spectral features in HCF is about 22:1.

III. OBSERVED SPECTRUM AND ANALYSIS

The high-resolution fluorooform plasma spectrum is recorded between 2613 and 2703 cm⁻¹, and the overview spectrum is given in Fig. 2. Previous experimental and theoretical work predicts that this region is dominated by the CH stretch vibration, ν_1 , of HCF.^{3,4,22} Preliminary analysis of the P- and R-branch spacing, ~2.2 cm⁻¹, indicates that three separate rovibrational bands of HCF can be recognized in the experimental spectrum, with band origins at ~2643.0, ~2568.3, and ~2645.5 cm⁻¹. Each rovibrational band is composed of multiple K_a -sub-bands with large spacings between sub-band Q-branches. Due to its molecular structure, HCF has a permanent dipole moment, as well as vibrational transition dipole moments, that lies in the plane of and between the a- and b-axes (Fig. 1). Consequently, the rovibrational bands of HCF are expected to have band structures composed of both a-type ($\Delta K_a = \text{even}$, $\Delta K_c = \text{odd}$) and b-type ($\Delta K_a = \text{odd}$, $\Delta K_c = \text{odd}$) transitions; we keep this historical a-type/b-type transition notation for the rest of this paper. The three rovibrational bands are color coded and their K_a -sub-band origins are marked by circles for a-type transitions and diamonds for b-type transitions in Fig. 2. The determined line positions and corresponding rotational assignments from our analysis

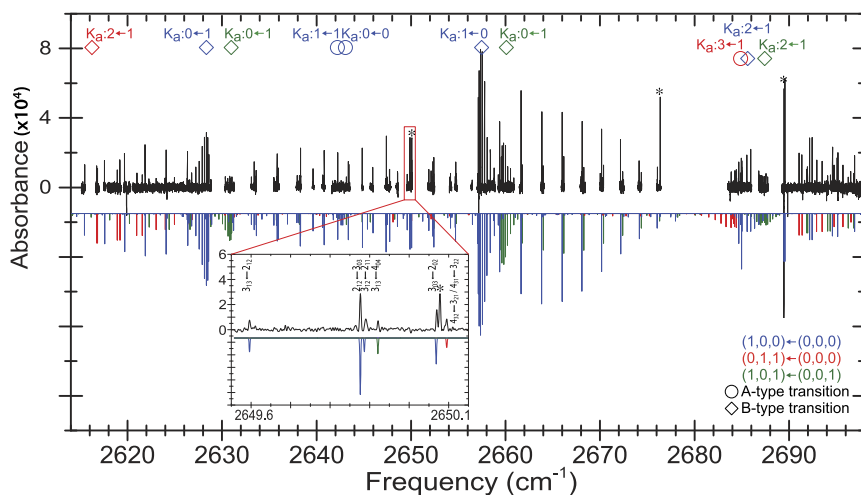


FIG. 2. The experimental spectrum (in black) of the fluorooform plasma products showing a series of rovibrational bands, with inverted simulated rovibrational bands of (1,0,0) ← (0,0,0) (in blue, using PGOPHER),²⁷ (0,1,1) ← (0,0,0) (in red), and (1,0,1) ← (0,0,1) (in green) plotted below to identify assigned transitions. The inset shows a blown-up region of the experimental and simulated spectra. The symbol (*) indicates unassigned lines.

TABLE II. Spectroscopic parameters^a (in cm⁻¹) of the HCF vibrational ground state.

	This work only	This work + Kakimoto ¹	Kakimoto, Saito, and Hirota ¹
A	15.562 22(38)	15.563 20(6)	15.562 70(37)
B	1.222 91(4)	1.223 05(4)	1.222 994(33)
C	1.129 86(3)	1.129 73(4)	1.129 678(33)
D _K (×10 ³)	2.34(7)	2.52(2)	2.43(6)
D _{JK} (×10 ⁴)	0.73(13)	0.84(19)	0.79(24)
D _J (×10 ⁶)	4.41(49)	4.50(8)	3.87(16)
δ _K (×10 ⁴)		0.53(2)	0.53(5)
δ _J (×10 ⁶)		0.31(1)	0.32(1)
H _K (×10 ⁵)		-0.25(19)	-0.47(25)
H _{KJ} (×10 ⁶)		0.46(24)	-0.10(17)
H _{JK} (×10 ⁸)		0 ^b	-0.40(47)
H _J (×10 ⁹)		0.47(21)	-0.63(33)

^aExperimental uncertainties are given in parentheses in units of the last significant digits.^bFixed to zero.

are given in the [supplementary material](#). In this spectral region, the (1,0,0) ← (0,0,0) band and the (0,1,1) ← (0,0,0) band are expected based on previous SEP measurements and analysis by Suzuki and Hirota.³

The rotational analysis of the observed bands is performed using the PGOPHER software,²⁷ starting from a Watson nonrigid asymmetric top Hamiltonian (A reduction and Ir representation). Vibrational assignments are then made based on the vibrational energies, ν_0 , and the primary rotational constants (A_v , B_v , and C_v). For newly reported vibrational states, the vibrationally dependent rotational constants, X_v , are estimated, to first order approximation, from

$$X_v = X_0 - \sum_i (\alpha_i^X \nu_i), \quad (1)$$

where α_i^X are the vibration-rotation interaction constants, ν_i is the vibrational quantum number, and X_0 represents A_0 , B_0 , and C_0 , which are the experimentally determined ground state values. From [Table I](#), it can be seen that the *ab initio* predicted α_i^X values for ν_1 and ν_2 are not in good agreement—particularly in sign—with previously reported experimental values. However, it was suggested in [Ref. 3](#) that the experimentally determined α_i constants are not the deperturbed values. As such, in our analysis, assignment of newly reported states is based on rotational constant estimates made using the *ab initio* predicted α_i^X values of [Ref. 4](#).

Spectral analyses of the bands are performed by fitting the observed transitions via least-squares analysis to determine tentative band origin, and lower and upper state rotational constants (A'' , B'' , C'' , A' , B' , and C' , respectively). These preliminary values are

TABLE III. Spectroscopic parameters^a (in cm⁻¹) of the observed vibrationally excited states of HCF.

	This work				Suzuki and Hirota ³	Mukarakate <i>et al.</i> ²²		
	(0,0,1)	(1,0,1)	(0,1,1)	(1,0,0)	(1,0,0)	(0,1,1)	(1,0,0)	(1,0,1)
ν_0	1 190.2(5)	3 835.7 ^b	2 568.337 5(3)	2 643.030 1(3)	2 643.039 3(26)	2568.3(5)	2642.9(5)	3835.7(5)
A	15.525 73(11)	15.207 54(4)	15.728 85(4)	15.229 74(7)	15.225 27(87)	15.74(4)	15.32(4)	15.21(4)
B	1.208 37(2)	1.211 42(3)	1.212 43(21)	1.221 75(7)	1.222 68(11)			
C	1.114 28(2)	1.109 60(2)	1.114 52(21)	1.124 91(7)	1.126 49(9)			
D _K (×10 ³)	0.26(18)	1.19(2)	3.46(1)	2.05(2)	1.43(5)			
D _{JK} (×10 ⁴)	2.44(1)	-2.68(6)	-0.07(2)	1.35(2)	3.39(7)			
D _J (×10 ⁶)	4.41(40)	6.40(50)	5.95(13)	2.90(7)	3.08(23)			
δ _K (×10 ⁴)	-0.30(20)	9.06(11)		-1.85(33)	0.53			
δ _J (×10 ⁶)	-3.02(88)	0.64(23)		-0.72(28)	0.39(24)			
ζ ^c			0.441 77(3)		0.317 8(34)			

^aExperimental uncertainties are given in parentheses in units of the last significant digits. The experimental frequency uncertainty is ± 0.0003 cm⁻¹.^bFixed to the value in [Ref. 22](#).

used to make vibrational assignments of the upper and lower states. With vibrational assignments made, systematic rotational analyses are carried out for each band; the analysis details for each individual band are provided in Secs. IV A–IV E, and the resulting spectroscopic parameters are summarized in Tables II and III. In addition to the expected $(1,0,0) \leftarrow (0,0,0)$ and $(0,1,1) \leftarrow (0,0,0)$ bands, the hot band $(1,0,1) \leftarrow (0,0,1)$ is assigned.

IV. DISCUSSION

A. Boltzmann analysis

Under the present slit jet expansion conditions, the HCF molecules are rotationally cold. Based on a Boltzmann analysis of the observed intensities (see Fig. 3), the rotational temperature of all rovibrational bands in the present experimental spectrum is determined to be 40.6 ± 1.3 K. It is noted, in the Boltzmann analysis of the rotational temperature, that only the transitions that do not show strong Coriolis mixing are considered. Conversely, the HCF molecules are vibrationally hot; the presence of the $(1,0,1) \leftarrow (0,0,1)$ band at this absorption intensity suggests a vibrational temperature of ~ 900 K. This mismatch between rotational and vibrational temperatures is a common feature of supersonic plasma discharges.^{28–31} Population of vibrationally excited states, starting from the lowest energy state, occurs via inelastic collisions with energetic electrons in the discharge, where energy is transferred to the molecule via vibration-translation (VT) energy transfer. The resulting vibrational temperature of the molecule increases in proportion to the high voltage applied.³⁰ In the case of HCF, the applied discharge

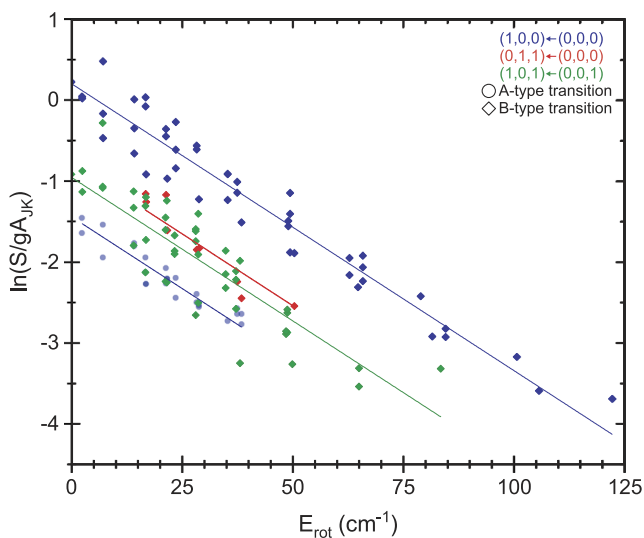


FIG. 3. Boltzmann analysis of the a-type (blue circles) and b-type (blue diamonds) transitions of the $(1,0,0) \leftarrow (0,0,0)$ band, the b-type (red diamonds) transitions of the $(0,1,1) \leftarrow (0,0,0)$ band, and the b-type (green diamonds) transitions of the $(1,0,1) \leftarrow (0,0,1)$ band of HCF, with y-intercepts of 0.21 ± 0.06 , -1.44 ± 0.06 , -0.76 ± 0.10 , and -0.95 ± 0.06 , respectively. Only the transitions that do not show strong Coriolis mixing are plotted and analyzed to determine the global rotational temperature, 40.6 ± 1.3 K.

voltage of ~ 7000 V/cm is sufficient to significantly populate the $(0,0,1)$ state at $1190.2(5) \text{ cm}^{-1}$. Other vibrationally excited states, e.g., the $(0,1,0)$ state at $1403.2045(13) \text{ cm}^{-1}$,³ could be expected to be populated at lower amounts. From Landau-Teller theory, VT relaxation in a supersonic expansion is typically only efficient for vibrations with energy at or below the collisional energy in the stagnation region, $kT/hc \sim 210 \text{ cm}^{-1}$. However, since the experimental buffer gas consists of the diatomic H_2 in addition to the monoatomic Ne and He, the efficiency of vibrational relaxation is likely increased for all energies and any population of vibrationally excited states would be significantly reduced.³² Consequently, at our current level of sensitivity, only the hot band out of the lowest energy state (ν_3) is observed.

B. The Coriolis coupled $(1,0,0) \leftarrow (0,0,0)$ and $(0,1,1) \leftarrow (0,0,0)$ bands

The strongest transitions in the experimental spectrum belong to the known CH stretch fundamental band, with a band origin at $2643.0393(26) \text{ cm}^{-1}$;³ the observed b-type Q-branches are shown in Fig. 4. The $(1,0,0) \leftarrow (0,0,0)$ band shows strong b-type transitions accompanied by weaker a-type transitions, and in total, five sub-bands are observed for the $(1,0,0) \leftarrow (0,0,0)$ vibrational transition: $K_a: 0 \leftarrow 1$, $K_a: 1 \leftarrow 0$, $K_a: 2 \leftarrow 1$, $K_a: 1 \leftarrow 1$, and $K_a: 0 \leftarrow 0$, three b-type and two a-type sub-bands, respectively. Due to selection rules and challenges of double resonance SEP spectroscopy, this is the first time both a- and b-type transitions for the $(1,0,0) \leftarrow (0,0,0)$ band have been observed. Based on the previously mentioned Boltzmann analysis of the $(1,0,0) \leftarrow (0,0,0)$ band intensities (Fig. 3), the ratio of the integrated intensities of the a- and b-type transitions, the CH stretch transition dipole moment is found to be $23.7(3)^\circ$ off the b-axis in a fixed body frame (Fig. 1).

The $(1,0,0)$ rovibrational manifold has been studied extensively by Suzuki and Hirota³ through electronic transitions using SEP spectroscopy and is noted to have strong Fermi interactions with two nearby states: the $(0,1,1)$ state, whose corresponding $(0,1,1) \leftarrow (0,0,0)$ band origin is redshifted just outside our difference frequency laser range, and the $(0,2,0)$ state, whose corresponding $(0,2,0) \leftarrow (0,0,0)$ band origin is substantial to the blue ($\sim 100 \text{ cm}^{-1}$) of the scanned spectral range. The initial fits of the band origin and principle rotational constants show that the progressions observed at around 2620 and 2690 cm^{-1} are consistent with the $(0,1,1) \leftarrow (0,0,0)$ band and can be assigned as the sub-bands: $K_a: 2 \leftarrow 1$ and $K_a: 3 \leftarrow 1$.^{3,22}

Notably, initial fits of the rotational parameters for the $(1,0,0) \leftarrow (0,0,0)$ and $(0,1,1) \leftarrow (0,0,0)$ bands, with a standard Hamiltonian, result in observed intensities and line positions that deviate strongly for $J' \geq 3$ transitions in the $(1,0,0) \leftarrow (0,0,0)$ $K_a: 2 \leftarrow 1$ and $(0,1,1) \leftarrow (0,0,0)$ $K_a: 3 \leftarrow 1$ sub-bands and deviate weakly for the Q-branch ($K'_c = J' - 1$) of the $(1,0,0) \leftarrow (0,0,0)$ $K_a: 1 \leftarrow 0$ sub-band. The SEP study of the $(1,0,0)$ fundamental by Suzuki and Hirota³ noted a c-type Coriolis interaction between the $(1,0,0)$ and $(0,1,1)$ vibrational states. Systematic rotational and perturbation analysis is performed here by simultaneous fitting of the $(1,0,0) \leftarrow (0,0,0)$ and $(0,1,1) \leftarrow (0,0,0)$ bands.

By combining transitions observed in our jet-cooled spectrum with LIF transitions by Kakimoto, Saito, and Hirota,¹ the ground

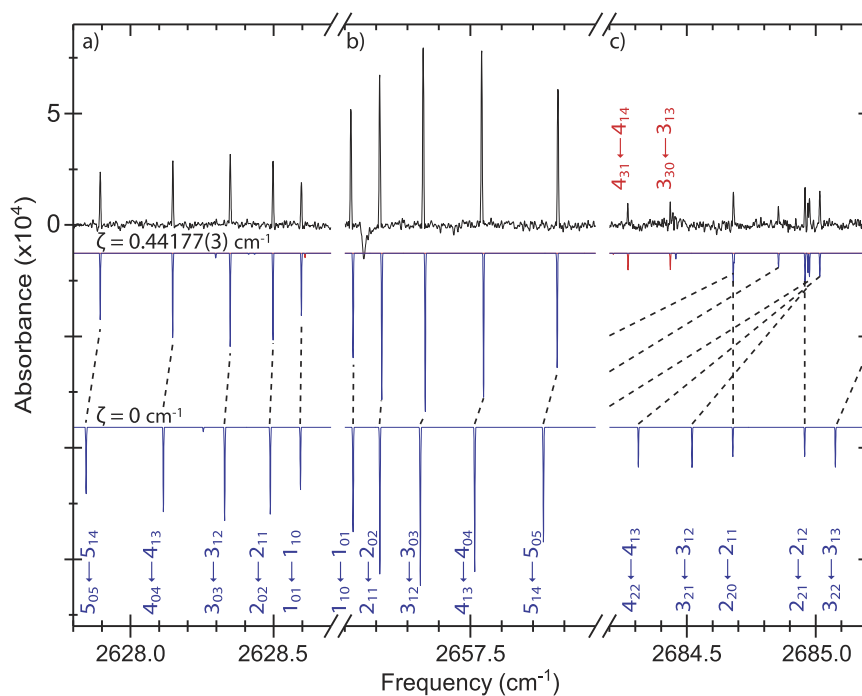


FIG. 4. The experimental spectrum (upper trace, in black) of $(1,0,0) \leftarrow (0,0,0)$ (in blue) and $(0,1,1) \leftarrow (0,0,0)$ (in red) Q-branch transitions with the inverted simulated spectra plotted below (using PGOPHER)²⁷ (middle trace) taking into account the effect of the Coriolis interaction and (lower trace) without the effect of the Coriolis interaction. The transition assignments of the $(1,0,0) \leftarrow (0,0,0)$ sub-band Q-branches appear along the bottom of the figure for (a) $K_a': 0 \leftarrow -1$, (b) $K_a': 1 \leftarrow 0$, and (c) $K_a': 2 \leftarrow 1$; the transition assignments of the $(0,1,1) \leftarrow (0,0,0)$ sub-band Q-branch appear along the top of the figure for (c) $K_a': 3 \leftarrow 1$.

state rotational constants are determined by lower state combination differences to be $A_0 = 15.563\,20(6)\text{ cm}^{-1}$, $B_0 = 1.223\,05(4)\text{ cm}^{-1}$, and $C_0 = 1.129\,73(4)\text{ cm}^{-1}$. These values are more precisely determined and in reasonable agreement (within 3σ) with the values determined by Kakimoto, Saito, and Hirota¹ and from the lower state combination difference analysis of the jet-cooled transitions alone (see Table II).

The upper state rotational constants for the $(1,0,0)$ and $(0,1,1)$ states are determined starting from the previously reported rotational constants of Suzuki and Hirota,³ including a Coriolis coupling constant, ζ^c , in the Hamiltonian, where the nondiagonal matrix elements of this coupling term are given by

$$\langle (0,1,1), J, K \pm 1 | H_{\text{corr}} | (1,0,0), J, K \rangle = \zeta^c \frac{1}{2} \sqrt{J(J+1) - K(K \pm 1)}. \quad (2)$$

C-type Coriolis interactions result from mixing angular momentum components that lie orthogonal to each other, e.g., the b-axis component of the $(1,0,0)$ vibration and the a-axis component of the $(0,1,1)$ vibration. Spectroscopically, c-type Coriolis mixing is only allowed between energy levels where $\Delta J = 0$, $\Delta K_a = \text{odd}$, and $\Delta K_c = \text{even}$. In the interest of simplicity, our rovibrational transition assignment scheme labels the mixed state as the original unperturbed state that is the majority component in the linear combination. In the experimental spectrum, the upper state assignments of the transition pairs that show the largest deviations (e.g., the $(1,0,0)$ $J', K_a', K_c' = 3, 2, 1$ state and the $(0,1,1)$ $J', K_a', K_c' = 3, 3, 1$ state) are consistent with and confirm that the $(1,0,0)$ and $(0,1,1)$ vibrational states mix through a c-type Coriolis interaction. A diagram of the rovibrational energy levels for the $(1,0,0)$ and $(0,1,1)$ vibrational

states based on the present experimental line positions is given in Fig. 5(a), which shows that the rotational energy levels of the two vibrationally excited states are highly intermixed. In particular, without the effects of the perturbation, the energies of the $K_a' = 2$ and $K_a' = 3$ levels of the $(1,0,0)$ and $(0,1,1)$ states, respectively, are predicted to be nearly degenerate [Fig. 5(b)].

The rotational parameters determined by Suzuki and Hirota,³ including their reported Coriolis coupling coefficient of $\zeta^c \sim 0.32\text{ cm}^{-1}$, do not reproduce the observed transition line positions for the highly affected $(1,0,0)$ $K_a' = 2$ and $(0,1,1)$ $K_a' = 3$ levels. Simultaneous least-squares fitting to a c-type Coriolis Hamiltonian of the transitions to the $(1,0,0)$ and $(0,1,1)$ states results in the best fit parameters, which are summarized in Table III. For the first time, the high precision vibrational energy and rotational constants of the $(0,1,1)$ state are determined to be $\nu_0 = 2568.3375(3)\text{ cm}^{-1}$, $A = 15.728\,85(4)\text{ cm}^{-1}$, $B = 1.212\,43(21)\text{ cm}^{-1}$, and $C = 1.114\,52(21)\text{ cm}^{-1}$, which are in agreement with the previous experimentally determined values and the predicted values for B and C.^{4,22} However, the spectroscopic parameters for the $(1,0,0)$ state are determined to be $\nu_0 = 2643.0301(3)\text{ cm}^{-1}$, $A = 15.229\,74(7)\text{ cm}^{-1}$, $B = 1.221\,75(7)\text{ cm}^{-1}$, $C = 1.124\,91(7)\text{ cm}^{-1}$, and $\zeta^c = 0.441\,77(3)\text{ cm}^{-1}$, which all significantly differ from those previously measured.^{3,22} Since all these parameters are related, our best assessment for the source of the discrepancies between the previous and current studies is that the SEP study did not observe transitions to the strongest Coriolis coupled states, e.g., they only observed transitions to the $(1,0,0)$ $K_a' = 2$ level with $J' = 2$.³

The best fit parameters are able to reproduce both the strong interaction seen for the $(1,0,0)$ $K_a' = 2$ and the $(0,1,1)$ $K_a' = 3$ levels and weaker interactions that affect the $(1,0,0)$ $K_a' < 2$ and the $(0,1,1)$ $K_a' < 3$ levels (see Fig. 4). As such, with the exception of the

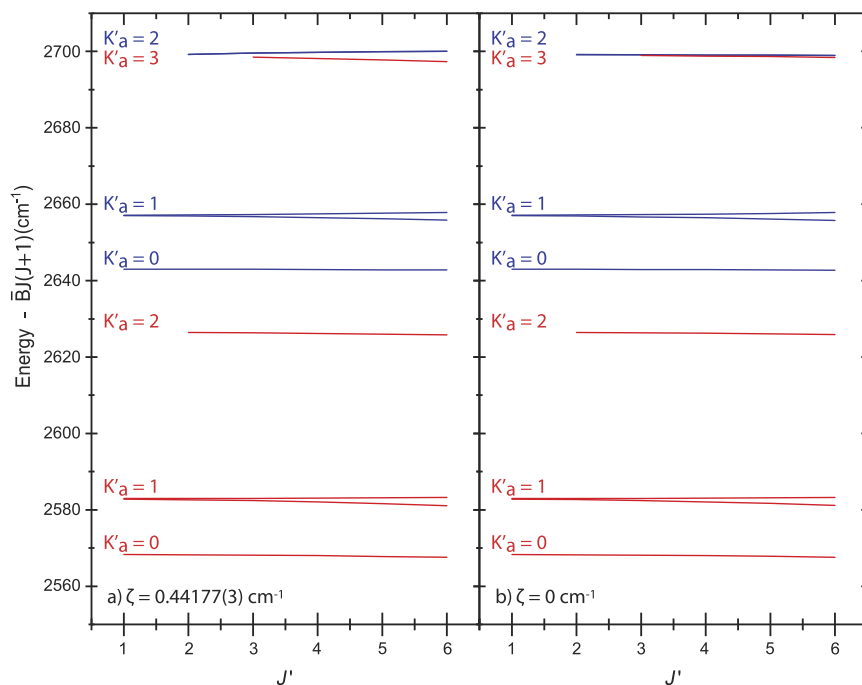


FIG. 5. The rovibrational energy levels of the (1,0,0) system (in blue) and the (0,1,1) system (in red), based on observed transitions and corrected for the \bar{B} rotational constant using the PGO-PHER software.²⁷ Note, in particular, the (1,0,0) $K'_a = 2$ and the (0,1,1) $K'_a = 3$ levels, which diverge in (a) due to the effect of the Coriolis interaction and are predicted to be nearly degenerate in (b) without the effect of the Coriolis interaction taken into account.

$K_a: 1 \leftarrow 0$ Q-branch transitions, the residuals for the fit (observed minus calculated, o – c, values) are reduced to about the experimental line position uncertainty, $\pm 0.0005 \text{ cm}^{-1}$. Given the finite scan range and CH stretch directed scope of this study, the possible Fermi

interactions between the (1,0,0), (0,1,1), and (0,2,0) states have not been considered in the rotational analysis and likely account for the larger o – c values measured for the (1,0,0) \leftarrow (0,0,0) $K_a: 1 \leftarrow 0$ Q-branch transitions.

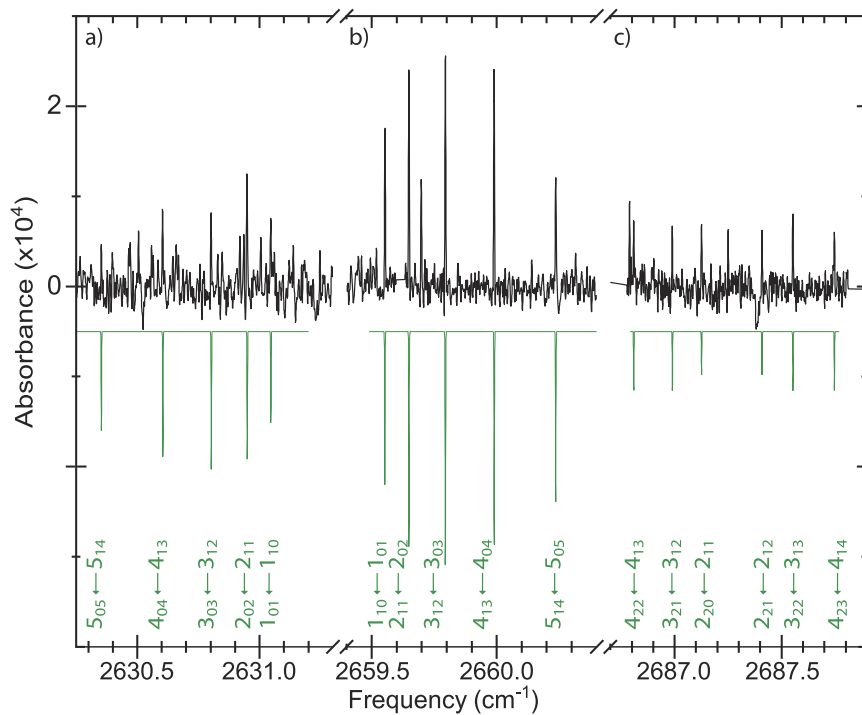


FIG. 6. The experimental spectrum (in black) of (1,0,1) \leftarrow (0,0,1) Q-branch transitions, with the inverted simulated spectra (in green, using PGO-PHER)²⁷ plotted below. The transition assignments appear along the bottom of the figure for (a) $K_a: 0 \leftarrow 1$, (b) $K_a: 1 \leftarrow 0$, and (c) $K_a: 2 \leftarrow 1$.

C. The (1,0,1) ← (0,0,1) hot band

A rovibrational band about 1/3 the observed intensity of the (1,0,0) ← (0,0,0) band is observed in the experimental spectrum, with a band origin at 2645.4589(3) cm⁻¹, that has not been previously reported. Only three b-type sub-bands are observed for this band: $K_a: 0 \leftarrow 1$, $K_a: 1 \leftarrow 0$, and $K_a: 2 \leftarrow 1$; the Q-branches are shown in Fig. 6. Based on the normal modes of HCF (see Table I), there are no additional bands, unaccounted for combination bands in this region, suggesting that it is a hot band. Moreover, given the close frequency proximity (~ 2.5 cm⁻¹) of the band origin to the (1,0,0) fundamental band origin, it is likely a hot band of the form $\nu_1 + \nu_x \leftarrow \nu_x$.

The best fit of the rotational parameters (Table III) results in, for example, primary rotational constants of $A'' = 15.52573(11)$ cm⁻¹ and $A' = 15.20754(4)$ cm⁻¹. From comparison with the SEP study by Mukarakate *et al.*,²² the upper state can be assigned as the (1,0,1) state, but the lower state matches none of the previously measured vibrational states. However, based on Eq. (1) and the *ab initio* α_i^X values of Weis *et al.*,⁴ the rotational constants for the (0,0,1) state are estimated to be $A_1 = 15.518$ cm⁻¹, $B_1 = 1.209$ cm⁻¹, and $C_1 = 1.114$ cm⁻¹. From these values, the lower state can be assigned as the (0,0,1) state. Furthermore, the determined rotational

parameters for the (1,0,1) ← (0,0,1) band are able to reproduce the transition line positions to within ± 0.0003 cm⁻¹, indicating the absence of any local perturbations.

This is the first observation of rotationally resolved data for the CF stretch (0,0,1) rovibrational manifold, whose vibrational energy is known to be 1192(2) cm⁻¹ from low resolution dispersed fluorescence spectroscopy by Fan *et al.*² However, hot bands can only provide energy differences between two vibrationally excited states. In order to more precisely determine the absolute vibrational energy, the data must be referenced to one of the vibrational manifolds. Since the energy of the (1,0,1) state (3835.7 cm⁻¹) is currently known to be of higher precision than the (0,0,1) state,²² the (1,0,1) state is used as the reference. Consequently, the (0,0,1) absolute vibrational energy, ν_0 , is determined to be 1190.2(5) cm⁻¹, which is in excellent agreement with the dispersed fluorescence results.²

D. Comparison with *ab initio* calculations

To support vibrational assignments, high-level *ab initio* calculations were carried out at the coupled-cluster with single, double, and perturbative triple [CCSD(T)] level of theory using the

TABLE IV. Harmonic and anharmonic (VPT2) frequencies^a (in cm⁻¹) and infrared intensities (in km/mol) of HCF fundamental and select combination bands.

	CCSD(T)/ANO2				CEPA ^b		Experimental ^c
	ω	Int.	ν	Int.	Pert. ν	Var. ν	ν
(0,0,1)	1214.4	164.6	1191.1	164.0	1190.6	1190.7	1190.2(5) ^d
(0,1,0)	1439.1	23.4	1405.8	21.2	1407.5	1406.9	1403.2045(13) ^e
(1,0,0)	2803.2	138.4	2641.1	94.7	2605.3	2640.7	2643.0300(3) ^d
(0,0,2)	2428.8		2362.7	3.2	2361.1	2361.5	2364.3(5) ^f
(0,1,1)	2653.5		2567.3	37.9	2580.3	2570.9	2568.3378(3) ^d
(0,2,0)	2878.2		2825.9	22.7	2846.2	2819.9	2812.4844(10) ^e
(0,1,2)	3867.9		3724.9	0.4	3733.1	3728.4	3729.4(5) ^f
(1,0,1)	4017.6		3834.2	0.1	3806.1	3834.8	3835.7(5) ^f
(1,1,0)	4242.3		3930.8	0.1	3900.7	3940.8	3936.5(5) ^f
(0,2,1)	4092.6		4024.6	1.9	4001.3	4023.3	4017.4(5) ^f
(0,3,0)	4317.3		4248.5	0.2	4316.1	4228.1	4220.7(5) ^f
(1,0,2)	5232.0		5004.3	0.03	4986.7	5009.0	5008.5(5) ^f
(2,0,0)	5606.3		5074.5	0.1	5067.7	5137.4	5134.7(5) ^f
(0,2,2)	5307.0		5130.2	0.01	5136.2	5214.3	5075.6(5) ^f
(1,2,0)	5681.4		5296.4	6.7	5227.3	5301.6	5295.6(5) ^f
(0,4,0)	5756.4		5630.3	0.0002	5817.1	5629.0	5617.3(5) ^f
(2,1,0)	7045.4		6388.4	0.03			6372.0(5) ^f
(1,3,0)	7120.5		6630.1	0.01			6640.1(5) ^f

^aAnharmonic zero-point energy (ZPE) = 2690.2 cm⁻¹.

^bReference 4.

^cExperimental uncertainties given in parentheses in units of the last significant digit.

^dThis work.

^eReference 3.

^fReference 22.

development version of the CFOUR program.³³ Anharmonic frequencies, infrared intensities, and vibrational corrections to the rotational constants have been determined from second-order vibrational perturbation theory (VPT2)³⁴ with full cubic and the semidiagonal part of the quartic force fields obtained by numerical differentiation of analytic CCSD(T) second derivatives computed using the frozen-core ANO2 basis set.^{35–37}

The harmonic and VPT2 fundamental frequencies of the fundamental and combination bands are summarized in Table IV. Comparison with experimental values shows that the present perturbative treatment better reproduces vibrational energies relative to the CEPA perturbative values, and for all but the $(0, \nu_2, 0)$ states is consistent with the CEPA variational calculations; however, the CEPA variational calculations are still the method of choice. Suzuki and Hirota³ observed a negative anharmonicity for ν_2 , which was assumed to be due to strong interactions between the $(1, 0, 0)$, $(0, 1, 1)$, and $(0, 2, 0)$ states. This interaction is further supported by the study of Weis *et al.*,⁴ which found poor agreement between the vibrational energies determined from variational and perturbative calculations. In order for the VPT2 fundamental frequencies to reproduce the experimental values, a combination of Fermi and Darling-Dennison interactions had to be addressed, where the vibrational frequencies as a result of such interactions are calculated by a deperturbation-diagonalization technique followed by transformation of the deperturbed transition moments.^{38,39}

In particular, analysis of the VPT2 fundamental frequencies shows that the $(0, \nu_2, 0)$ states mix, to some extent, with all nearby states (within a few hundred cm^{-1}), except for $(0, 0, \nu_3)$ states. For example, the VPT2 fundamental frequency of 2641.1 cm^{-1} for the $(1, 0, 0)$ state is determined by including Fermi interactions between the $(1, 0, 0)$, $(0, 1, 1)$, and $(0, 2, 0)$ vibrational states, with an interaction constant $\sim 34.6 \text{ cm}^{-1}$ between $(1, 0, 0)$ and $(0, 1, 1)$; $\sim 52.0 \text{ cm}^{-1}$ between $(1, 0, 0)$ and $(0, 2, 0)$; and $\sim 2.1 \text{ cm}^{-1}$ between $(0, 1, 1)$ and $(0, 2, 0)$. If these interactions were not accounted for, the anharmonic frequency of the $(1, 0, 0)$ state is predicted to be

2607.3 cm^{-1} , about 40 cm^{-1} below the experimentally observed band origin. Correspondingly, the interactions shift the $(0, 1, 1)$ predicted energy from 2579.8 to 2567.3 cm^{-1} and the $(0, 2, 0)$ energy from 2847.1 to 2825.9 cm^{-1} . Of particular relevance, the mixing of the $(0, 1, 1)$, $(1, 0, 0)$, and $(0, 2, 0)$ states results in significant infrared intensity borrowing, with the predicted IR intensity of the $(0, 1, 1) \leftarrow (0, 0, 0)$ band increasing from about 7.1 to 37.9 km/mol , the $(1, 0, 0) \leftarrow (0, 0, 0)$ band increasing from about 68.5 to 94.7 km/mol , and the $(0, 2, 0) \leftarrow (0, 0, 0)$ band decreasing from 91.5 to 22.7 km/mol . In the present experiment, all observed $(0, 1, 1) \leftarrow (0, 0, 0)$ transitions originate from $K_d'' = 1$ levels, which should be sparsely populated at the low rotational temperature of the slit jet expansion. As such, the fact that these transitions are observed in the jet-cooled experimental spectrum is evidence of significant intensity borrowing and suggests the presence of the VPT2 predicted resonances.

The strong mixing between states is further reflected in the experimentally determined vibration-rotation interaction constants, α_i . The VPT2 α_i values, given in Table V, are consistent in both sign and magnitude to those predicted by the CEPA calculations, e.g., the VPT2 $\alpha_1^A = 0.611 \text{ cm}^{-1}$ and the CEPA $\alpha_1^A = 0.623 \text{ cm}^{-1}$.⁴ The VPT2 α_i values do not include effects due to state mixing and as such will be in agreement with the experimental deperturbed values. Using Eq. (1), the experimental α_i values can be determined two ways: (1) from the rotational constants of the upper state of the fundamental bands and (2) from the rotational constants of combination states, where the α_i not to be determined is fixed to the value determined from its fundamental bands; the results are summarized in Table V. It is expected that if the perturbative effects to a particular state are accounted for in determining experimental rotational constants, then the resulting α_i should be of the same magnitude and sign, regardless of whether it was determined from fundamental or combination state values. The vibration-rotation interaction constants for the CF vibrational mode, ν_3 , are experimentally determined for the first time from the $(0, 0, 1)$ rotational constants to be $\alpha_3^A = 0.0375(1)$, $\alpha_3^B = 0.01468(4)$, and

TABLE V. Experimental and theoretical vibration-rotation interaction constants, α_i (in cm^{-1}), of HCF.^c

		α_i^A	α_i^B	α_i^C
	Method	($\times 10^2$)	($\times 10^2$)	($\times 10^2$)
(0,0,1)	CCSD(T)/ANO2	4.55	1.43	1.54
	Eخت. from (0,0,1) ^a	3.75(1)	1.468(4)	1.545(4)
	Eخت. from (1,0,1) ^a	2.22(1)	1.03(1)	1.53(1)
(0,1,0)	CCSD(T)/ANO2	-36.0	0.024	0.540
	Eخت. from (0,1,0) ^b	-37.21(2)	-0.03(1)	0.53(1)
	Eخت. from (0,2,0) ^b	-31.35(2)	-0.03(1)	0.50(1)
	Eخت. from (0,1,1) ^a	-20.31(1)	-0.41(2)	-0.02(2)
(1,0,0)	CCSD(T)/ANO2	61.1	-0.281	-0.043
	Eخت. from (1,0,0) ^a	33.35(1)	0.13(1)	0.48(1)
	Eخت. from (1,0,1) ^a	31.82(1)	-0.31(1)	0.47(1)

^aBased on experimental rotational constants from this work.

^bBased on experimental rotational constants from Ref. 3.

^cRegular and italic font correspond to theoretically and experimentally derived values, respectively.

TABLE VI. Predicted pure rotational transitions of HCF.

J'	K_a'	K_c'		J''	K_a''	K_c''	Position (MHz)
2	0	2	–	1	0	1	141 051(9)
2	1	1	–	1	1	0	143 845(9)
3	0	3	–	2	0	2	211 535(9)
4	0	4	–	3	0	3	281 968(9)
5	0	5	–	4	0	4	352 335(9)

$\alpha_3^C = 0.01545(4) \text{ cm}^{-1}$; these are in good agreement with the *ab initio* predicted values. However, the vibration-rotation interaction constants for ν_1 and ν_2 exhibit erratic behavior relative to the predicted values whether extracted from fundamental or combination state experimental rotational constants, e.g., differing in sign for α^B and α^C . This suggests that all perturbative effects to these states [e.g., the (1,0,0) state] are still not fully accounted for, and these experimentally determined spectroscopic constants are not the fully deperturbed values.

E. Spectroscopic predictions

The vibrational energies and rotational constants determined from this work are sufficiently precise to predict the lowest energy transitions of HCF, which could aid its detection in laboratory or astronomical spectra. Most importantly, the ground state rotational constants presented here from the combined fit of IR and SEP data offer the most reliable prediction of pure rotational transitions; examples of such microwave transitions expected to be strong at interstellar temperatures ($\sim 20 \text{ K}$) are given in Table VI. Similarly, the present experimentally determined ground and (0,0,1) state spectroscopic parameters allow for accurate prediction of the lowest energy vibrational transition—the CF fundamental band (see Table VII for predicted Q-branch transitions). Based on the transition frequencies, HCF should be spectroscopically accessible through astronomical observation of pure rotational transitions or rovibrational

TABLE VII. Predicted Q-branch transitions of HCF (0,0,1) fundamental vibration.

J'	K_a'	K_c'		J''	K_a''	K_c''	Position (cm^{-1})
1	1	0	–	1	1	1	1190.2842(3)
2	1	1	–	2	1	2	1190.4107(3)
3	1	2	–	3	1	3	1190.6006(3)
1	1	1	–	1	1	0	1190.0968(3)
2	2	0	–	2	2	1	1190.0939(3)
2	2	1	–	2	2	0	1190.0930(3)
2	1	2	–	2	1	1	1189.8485(3)
1	1	0	–	1	0	1	1204.6217(3)
2	1	1	–	2	0	2	1204.6552(3)
3	1	2	–	3	0	3	1204.7065(3)
1	0	1	–	1	1	0	1175.7803(3)
2	0	2	–	2	1	1	1175.6268(3)
3	0	3	–	3	1	2	1175.3957(3)

transitions with instruments such as the Atacama Large Millimeter/submillimeter Array (ALMA) and the James Webb Space Telescope (JWST), respectively.

V. CONCLUSION

Five vibrational states of jet-cooled HCF have been investigated using high-resolution direct infrared absorption spectroscopy, for three of which the rotational constants are reported for the first time. Detailed and systematic rotational analyses of the observed rovibrational bands are presented, resulting in accurate spectroscopic parameters for the (0,0,0), (0,0,1), (0,1,1), (1,0,0), and (1,0,1) vibrational states and significantly extending the available rovibrational data for the HCF molecule.

A detailed perturbation analysis of the c-type Coriolis interaction between the (1,0,0) and (0,1,1) vibrational manifolds sheds new light on the rovibrational coupling in HCF and provides an improvement on the previous spectroscopic parameters for both states. Most dramatically, the strong interaction between the $K_a' = 2$ and $K_a' = 3$ levels of the (1,0,0) and (0,1,1) states, respectively, has been analyzed completely. While not directly addressed in the present experimental rovibrational study, comparison of the experimental spectral intensities and band origins with those predicted from *ab initio* calculations further supports the claim of strong Fermi interactions between the (1,0,0), (0,1,1), and (0,2,0) states.

SUPPLEMENTARY MATERIAL

See the [supplementary material](#) for the complete line lists with observed minus calculated (o – c) values obtained from the spectral fitting of the experimental spectrum using the PGOPHER software.²⁷

ACKNOWLEDGMENTS

This work was supported by grants from the Department of Energy (Grant No. DE-FG02-09ER16021), with initial funds for construction of the slit-jet laser spectrometer provided by the National Science Foundation (Grant Nos. CHE-1665271 and PHY 1734006). K.D.D. would like to thank Dr. N. Ligterink for helpful discussions and the NIST NRC Postdoctoral Research Associateship Program for financial support.

REFERENCES

- M. Kakimoto, S. Saito, and E. Hirota, “Doppler-limited dye laser excitation spectroscopy of HCF,” *J. Mol. Spectrosc.* **88**, 300–310 (1981).
- H. Fan, C. Mukarakate, M. Deselnicu, C. Tao, and S. A. Reid, “Dispersed fluorescence spectroscopy of jet-cooled HCF and DCF: Vibrational structure of the \tilde{X}^1A' state,” *J. Chem. Phys.* **123**, 014314 (2005).
- T. Suzuki and E. Hirota, “Optical-optical double resonance (stimulated emission pumping) spectroscopy of HCF,” *J. Chem. Phys.* **88**, 6778–6784 (1988).
- B. Weis, P. Rosmus, K. Yamashita, and K. Morokuma, “Theoretical potential energy and electric dipole moment functions of HCF (X^1A' and a^3A'),” *J. Chem. Phys.* **92**, 6635–6644 (1990).
- S. Elliot and F. S. Rowland, “Chlorofluorocarbons and stratospheric ozone,” *J. Chem. Educ.* **64**, 387 (1987).
- W. Kirmse, *Carbene Chemistry* (Elsevier, 2013), Vol. 1.
- K. Acharyya and E. Herbst, “Gas-grain fluorine and chlorine chemistry in the interstellar medium,” *Astrophys. J.* **850**, 105 (2017).

- ⁸E. W. Schwietzman, N. Y. Kiang, M. N. Parenteau, C. E. Harman, S. DasSarma, T. M. Fisher, G. N. Arney, H. E. Hartnett, C. T. Reinhard, S. L. Olson, V. S. Meadows, C. S. Cockell, S. I. Walker, J. L. Grenfell, S. Hegde, S. Rugheimer, R. Hu, and T. W. Lyons, "Exoplanet biosignatures: A review of remotely detectable signs of life," *Astrobiology* **18**, 663–708 (2018).
- ⁹E. C. Fayolle, K. I. Öberg, J. K. Jørgensen, K. Altwegg, H. Calcutt, H. S. P. Müller, M. Rubin, M. H. D. van der Wiel, P. Bjerkeli, T. L. Bourke, A. Coutens, E. F. van Dishoeck, M. N. Drozdovskaya, R. T. Garrod, N. F. W. Ligterink, M. V. Persson, S. F. Wampfler, H. Balsiger, J. J. Berthelier, J. De Keyser, B. Fiethe, S. A. Fuselier, S. Gasc, T. I. Gombosi, T. Sémon, C. Y. Tzou, and ROSINA Team, "Protostellar and cometary detections of organohalogens," *Nat. Astron.* **1**, 703–708 (2017).
- ¹⁰M. Kama, E. Caux, A. López-Sepulcre, V. Wakelam, C. Dominik, C. Ceccarelli, M. Lanza, F. Lique, B. B. Ochsendorf, D. C. Lis, R. N. Caballero, and A. G. G. M. Tielens, "Depletion of chlorine into HCl ice in a protostellar core—The CHESSE spectral survey of OMC-2 FIR 4," *Astron. Astrophys.* **574**, A107 (2015).
- ¹¹D. A. Neufeld, J. Zmuidzinas, P. Schilke, and T. G. Phillips, "Discovery of interstellar hydrogen fluoride," *Astrophys. J., Lett.* **488**, L141–L144 (1997); e-print [arXiv:astro-ph/9708013](https://arxiv.org/abs/astro-ph/9708013).
- ¹²D. A. Neufeld, P. Schilke, K. M. Menten, M. G. Wolfire, J. H. Black, F. Schuller, H. S. P. Müller, S. Thorwirth, R. Güsten, and S. Philipp, "Discovery of interstellar CF⁺," *Astron. Astrophys.* **454**, L37–L40 (2006).
- ¹³T. G. Phillips, E. A. Bergin, D. C. Lis, D. A. Neufeld, T. A. Bell, S. Wang, N. R. Crockett, M. Emprechtinger, G. A. Blake, E. Caux, C. Ceccarelli, J. Cernicharo, C. Comito, F. Daniel, M.-L. Dubernet, P. Encrenaz, M. Gerin, T. F. Giesen, J. R. Goicoechea, P. F. Goldsmith, E. Herbst, C. Joblin, D. Johnstone, W. D. Langer, W. D. Latter, S. D. Lord, S. Maret, P. G. Martin, G. J. Melnick, K. M. Menten, P. Morris, H. S. P. Müller, J. A. Murphy, V. Ossenkopf, J. C. Pearson, M. Pérault, R. Plume, S.-L. Qin, P. Schilke, S. Schlemmer, J. Stutzki, N. Trappe, F. F. S. van der Tak, C. Vastel, H. W. Yorke, S. Yu, J. Zmuidzinas, A. Boogert, R. Güsten, P. Hartogh, N. Honingh, A. Karpov, J. Kooi, J.-M. Krieg, and R. Schieder, "Herschel observations of EXtra-Ordinary Sources (HEXOS): Detection of hydrogen fluoride in absorption towards Orion KL," *Astron. Astrophys.* **518**, L109 (2010); e-print [arXiv:1007.2149](https://arxiv.org/abs/1007.2149).
- ¹⁴P. Sonnentrucker, M. Wolfire, D. A. Neufeld, N. Flagey, M. Gerin, P. Goldsmith, D. Lis, and R. Monje, "A Herschel/HIFI legacy survey of HF and H₂O in the galaxy: Probing diffuse molecular cloud chemistry," *Astrophys. J.* **806**, 49 (2015).
- ¹⁵J. Cernicharo and M. Guelin, "Metals in IRC +10216—Detection of NaCl, AlCl, and KCl, and tentative detection of AlF," *Astron. Astrophys.* **183**, L10–L12 (1987).
- ¹⁶M. Agúndez, J. Cernicharo, L. B. F. M. Waters, L. Decin, P. Encrenaz, D. Neufeld, D. Teyssier, and F. Daniel, "HIFI detection of hydrogen fluoride in the carbon star envelope IRC +10216," *Astron. Astrophys.* **533**, L6 (2011).
- ¹⁷N. Indriolo, D. A. Neufeld, A. Seifahrt, and M. J. Richter, "Direct determination of the HF/H₂ abundance ratio in interstellar gas," *Astrophys. J.* **764**, 188 (2013).
- ¹⁸M. Asplund, N. Grevesse, A. J. Sauval, and P. Scott, "The chemical composition of the sun," *Annu. Rev. Astron. Astrophys.* **47**, 481–522 (2009).
- ¹⁹A. J. Merer and D. N. Travis, "Rotational analysis of bands of the HCF molecules," *Can. J. Phys.* **44**, 1541–1550 (1966).
- ²⁰H. Fan, I. Ionescu, C. Annesley, and S. A. Reid, "Lifetime lengthening and the Renner-Teller effect in the HCF ($\tilde{A}^1A'' \leftarrow \tilde{X}^1A'$) system," *Chem. Phys. Lett.* **378**, 548–552 (2003).
- ²¹H. Fan, I. Ionescu, C. Annesley, J. Cummins, M. Bowers, J. Xin, and S. A. Reid, "On the Renner-Teller effect and barriers to linearity and dissociation in HCF (\tilde{A}^1A'')," *J. Phys. Chem. A* **108**, 3732–3738 (2004).
- ²²C. Mukarakate, C. Tao, C. D. Jordan, W. F. Polik, and S. A. Reid, "Stimulated emission pumping spectroscopy of the $\tilde{X}A'$ state of CHF," *J. Phys. Chem. A* **112**, 466–471 (2008).
- ²³S. Davis, M. Fárník, D. Uy, and D. J. Nesbitt, "Concentration modulation spectroscopy with a pulsed slit supersonic discharge expansion source," *Chem. Phys. Lett.* **344**, 23–30 (2001).
- ²⁴A. Kortyna and D. J. Nesbitt, "Infrared spectroscopy of jet-cooled HCCl singlet chlorocarbene diradical: CH stretching and vibrational coupling dynamics," *J. Chem. Phys.* **149**, 074303 (2018).
- ²⁵T. M. Niebauer, J. E. Faller, H. M. Godwin, J. L. Hall, and R. L. Barger, "Frequency stability measurements on polarization-stabilized He–Ne lasers," *Appl. Opt.* **27**, 1285–1289 (1988).
- ²⁶C. Rinsland, M. Smith, A. Goldman, V. Devi, and D. Benner, "The fundamental bands of H³⁵Cl and H³⁷Cl: Line positions from high-resolution laboratory data," *J. Mol. Spectrosc.* **159**, 274–278 (1993).
- ²⁷C. M. Western, PGOPHER version 10.1, 2018, University of Bristol Research Data Repository.
- ²⁸G. Scoles, *Atomic and Molecular Beam Methods* (Oxford University Press, 1988).
- ²⁹J.-U. Grabow, N. Heineking, and W. Stahl, "A molecular beam microwave Fourier transform (MB-MWFT) spectrometer with an electric discharge nozzle," *Z. Naturforsch., A* **46**, 914–916 (1991).
- ³⁰M. E. Sanz, M. C. McCarthy, and P. Thaddeus, "Vibrational excitation and relaxation of five polyatomic molecules in an electrical discharge," *J. Chem. Phys.* **122**, 194319 (2005).
- ³¹D. Zhao, K. D. Doney, and H. Linnartz, "High-resolution infrared spectra of vibrationally excited HC₄H in a supersonic hydrocarbon plasma jet," *J. Mol. Spectrosc.* **296**, 1–8 (2014).
- ³²G. M. McClelland, K. L. Saenger, J. J. Valentini, and D. R. Herschbach, "Vibrational and rotational relaxation of iodine in seeded supersonic beams," *J. Phys. Chem.* **83**, 947–959 (1979).
- ³³CFOUR, 2017, Coupled-Cluster techniques for Computational Chemistry, a quantum-chemical program package by J. F. Stanton, J. Gauss, M. E. Harding, P. G. Szalay with contributions from A. A. Auer, R. J. Bartlett, U. Benedikt, C. Berger, D. E. Bernholdt, Y. J. Bomble, L. Cheng, O. Christiansen, F. Engel, R. Faber, M. Heckert, O. Heun, C. Huber, T.-C. Jagau, D. Jonsson, J. Jusélius, K. Klein, W. J. Lauderdale, F. Lipparini, D. A. Matthews, T. Metzroth, L. A. Mück, D. P. O'Neill, D. R. Price, E. Prochnow, C. Puzzarini, K. Ruud, F. Schiffmann, W. Schwalbach, C. Simmons, S. Stopkowitz, A. Tajti, J. Vázquez, F. Wang, J. D. Watts and the integral packages MOLECULE (J. Almlöf and P. R. Taylor), PROPS (P. R. Taylor), ABACUS (T. Helgaker, H. J. Aa. Jensen, P. Jørgensen, and J. Olsen), and ECP routines by A. V. Mitin and C. van Wüllen, for the current version, see <http://www.cfour.de>.
- ³⁴I. M. Mills, *3,2 Vibration-Rotation Structure in Asymmetric-and Symmetric-Top Molecules* (Academic Press, 1972), Vol. 1, p. 115.
- ³⁵J. Almlöf and P. R. Taylor, "General contraction of Gaussian basis sets. I. Atomic natural orbitals for first- and second-row atoms," *J. Chem. Phys.* **86**, 4070–4077 (1987).
- ³⁶D. Feller, "The role of databases in support of computational chemistry calculations," *J. Comput. Chem.* **17**, 1571–1586 (1996).
- ³⁷K. L. Schuchardt, B. T. Didier, T. Elsethagen, L. Sun, V. Gurumoorthi, J. Chase, J. Li, and T. L. Windus, "Basis set exchange: A community database for computational sciences," *J. Chem. Inf. Model.* **47**, 1045–1052 (2007).
- ³⁸J. Vázquez and J. F. Stanton, "Treatment of Fermi resonance effects on transition moments in vibrational perturbation theory," *Mol. Phys.* **105**, 101–109 (2007).
- ³⁹D. A. Matthews, J. Vázquez, and J. F. Stanton, "Calculated stretching overtone levels and Darling-Dennison resonances in water: A triumph of simple theoretical approaches," *Mol. Phys.* **105**, 2659–2666 (2007).